A chronosequence of human remains on soil microbial populations

Jason K Reynolds*, Natasha Robinson[1], Rani Carroll[1], Maiken Ueland[2], Thomas C Jeffries[1] & Hayley Green[1]

[1]School of Science, Western Sydney University, Locked Bag 1797, Penrith, NSW, 2751, Australia
[2]Center for Forensic Science, School of Mathematical and Physical Sciences, University of Technology Sydney, Sydney, NSW, 2007, Australia
*Corresponding author: j.reynolds@westernsydney.edu.au

Abstract

Surficial human decomposition produces substantial and measurable shifts in soil chemistry and microbial composition. This decade-long investigation examined temporal changes beneath surface deposited human remains and identified strong microbial and chemical responses in the first twelve to twenty four months, including decreased microbial diversity, elevated soil nutrients and sustained increases in several trace elements. Sequencing of the 16S rRNA V4 region showed increases in abundance of Gammaproteobacteria and Actinomycetes and decreases in Verrucomicrobiae and Planctomycetia during the first six to twelve months postmortem followed by a return towards control soil levels. Pseudomonadota (c. Alphabacteria) and Acidobacteria (c. Terriglobia) peaked in late decomposition stages after initial decreases during active decomposition. Initial soil pH and exchangeable base cations increased with a return of exchangeable aluminium after 5 years. Total and DTPA zinc increased after 3 years and remained elevated and did not return to baseline levels after nine years. Redundancy analysis demonstrated that microbial patterns in the first few years are tightly linked to elevated nutrients and trace elements, but these associations weaken as nutrient pools decline and responsive taxa diminish. Older cohorts retained a modest soil chemical signature and by approximately eight years both chemistry and microbial communities converged toward baseline. These findings show that soils preserve a long lived decomposition imprint and support the potential to extend postmortem interval estimation beyond active decomposition.

Keywords

Forensics, post mortem interval, microbial biodiversity, 16S rDNA

Highlights

- Soil microbial diversity measures are useful for PMI estimation for time scales to <2 years .
- Selective and total elemental loads including Zn can be used for PMI estimations >2 years.
- Soil chemical and biological condition may approach a return to baseline conditions >8 years.

1. Introduction

Decomposition of human remains drives a series of biological, chemical, and ecological processes that transform the surrounding soil environment. On a soil, the area directly beneath and adjacent to a cadaver becomes enriched in organic matter, nutrients, and microbial biomass derived from soft-tissue breakdown (Aitkenhead-Peterson et al., 2012; Carter et al., 2007; Taylor et al., 2023). These localised cadaver decomposition islands form transient nutrient hotspots characterised by elevated concentrations of ammonium, phosphate, dissolved organic carbon, and soluble elements including sodium, potassium, sulfur, and phosphorus (Taylor et al., 2023; Zhang et al., 2021). Such enrichment modifies nutrient availability, pH, and electrical conductivity, stimulates microbial activity, and generates steep biogeochemical gradients relative to surrounding soils (Aitkenhead-Peterson et al., 2012; Taylor et al., 2024).

Successive microbial and chemical transformations accompany these changes. The rapid influx of necromass promotes microbial proliferation and predictable community shifts that reflect decomposition stage (Guo et al., 2016; Metcalf et al., 2013). Early stages are dominated by taxa utilising protein- and lipid-rich substrates, including *Firmicutes*, *Bacteroidetes*, and *Proteobacteria*, followed by a transition to anaerobic and fermentative groups as oxygen becomes depleted (Metcalf et al., 2013; Guo et al., 2016). These reproducible trajectories underpin the concept of a microbial clock capable of estimating post-mortem interval (PMI) (Cobaugh et al., 2015; Metcalf et al., 2013). Fungal and micro-eukaryotic responses remain less well characterised but offer potential as complementary indicators of decomposition stage (Taylor et al., 2024).

Environmental context strongly mediates these processes. Soil texture, moisture, temperature, and exposure condition influence oxygen diffusion, drainage, and nutrient mobility, altering decomposition rates and community composition (Jaggers et al., 2009; Zhang et al., 2021). Clay-rich or compacted soils restrict aeration and delay tissue breakdown (Jaggers et al., 2009). Integrating such site variables into microbial-based PMI models improves predictive accuracy within local environmental contexts (Mason et al., 2024; Taylor et al., 2024). Microbial succession is linked to concurrent shifts in soil geochemistry and Taylor et al. (2023) identified three pathways during human decomposition: direct release of tissue-derived solutes (Na, K, P, S), secondary mobilisation of Ca, Mg, and Mn through cation exchange and acid solubilisation, and dissolution of Fe–Al oxides under acidifying conditions. These findings complement later observations that decomposition induces transient hypoxia, altered nitrogen cycling, and sustained changes in soil respiration and pH for at least one year (Taylor et al., 2024). Collectively, these studies demonstrate that microbial and abiotic responses are tightly coupled and together shape the long-term legacy of decomposition in soils.

Despite this progress, the persistence of biogeochemical and microbial signatures over decadal timescales remains poorly understood. Determining how long such indicators endure is critical for extending PMI estimation frameworks and for understanding the ecological consequences of human decomposition. This study investigates changes in soil chemistry and microbial community structure beneath decomposing human remains over a ten-year period at the Australian Taphonomic Research Facility (AFTER). By analysing both short-term and long-term transformations, we aim to identify persistent soil indicators that support forensic estimation of the post-mortem interval. This approach contributes to decomposition-based forensic models rooted in measurable soil processes and expands understanding of how necromass is incorporated into soil ecosystems.

This study explored human-remain decomposition over a ten-year period at the Australian Facility for Taphonomic Experimental Research (AFTER) site to understand soil chemical and biological changes over extended time frames. The questions that were investigated were: (1) what is the soil microbial ecological and geochemical response during human decomposition? (2) how long are these responses sustained in the soil environment? and (3) does the soil return to baseline conditions within a ten-year period.

2. Materials and Methods

2.1 Study site

The Australian Taphonomic Research (AFTER) site, west of Sydney, NSW (33°35'12.9"S 150°22'14.6"E), covers 1.03 ha of secured but otherwise open eucalypt woodland under restricted access arrangement. The site resides on the undulating Hawkesbury Sandstone lower slopes of the Blue Mountains region approaching the Hawkesbury-Nepean river system. Wianamatta Group sandstone, siltstone and shale are present on the edges of the site. The AFTER facility resides on altitudes of 40-50 m (Belmer et al., 2015; Fryirs et al., 2021). The site has a temperate climate, with a mean daily maximum temperature of 31°C, a minimum of 4°C, and 781 mm of precipitation per year (Bureau of Meteorology, 2025). A period of drought persisted through 2017 to 2020 with extended periods of low rainfall and high temperatures in the region. From 2020 to sample collection in 2025 there has been increased rainfall in response to ENSO and SOI shifts.

Soils at the study area are mapped as kurosols, and downslope as tenosols (NSW DPIE, 2025) under the Australian Soil Classification system (Isbell et al., 2021) and are generally shallow to moderately deep (30–100 cm) Yellow Earths and Earthy Sands. At the surface a loamy sand to sandy loam is present with loose, apedal single grained structure and porous sandy fabric. It occurs as topsoil (A1 horizon). The colour often becomes lighter with depth and ranges from dull yellowish brown (10YR 5/3), when organic matter is present, to brown (10YR 4/4). The pH varies from strongly acid (pH 4.5) to slightly acid (pH 5.5). Small sandstone and platy ironstone fragments, charcoal fragments and roots are common. Iron-cemented sandstone fragments with 7.5R 4/4 hematitic cores and yellow goethitic margins occur within red kaolinitic colluvium on a midslope bench above the Hawkesbury–Nepean River. They formed during Tertiary deep weathering of Hawkesbury Sandstone and were later reworked into mixed colluvial and fluvial slope deposits. In some sections of the study site this surface layer is not present and a yellowish brown clayey sand with apedal massive structure and porous earthy fabric is present. It generally occurs as subsoil over sandstone bedrock. Where it is exposed at the surface it forms a hardsetting topsoil and texture may increase to a light sandy clay loam with depth. Colour is yellowish brown (10YR 6/8) and red and orange mottles are occasionally present with depth. The pH varies from strongly acid (pH 4.0) to slightly acid (pH 6.5).

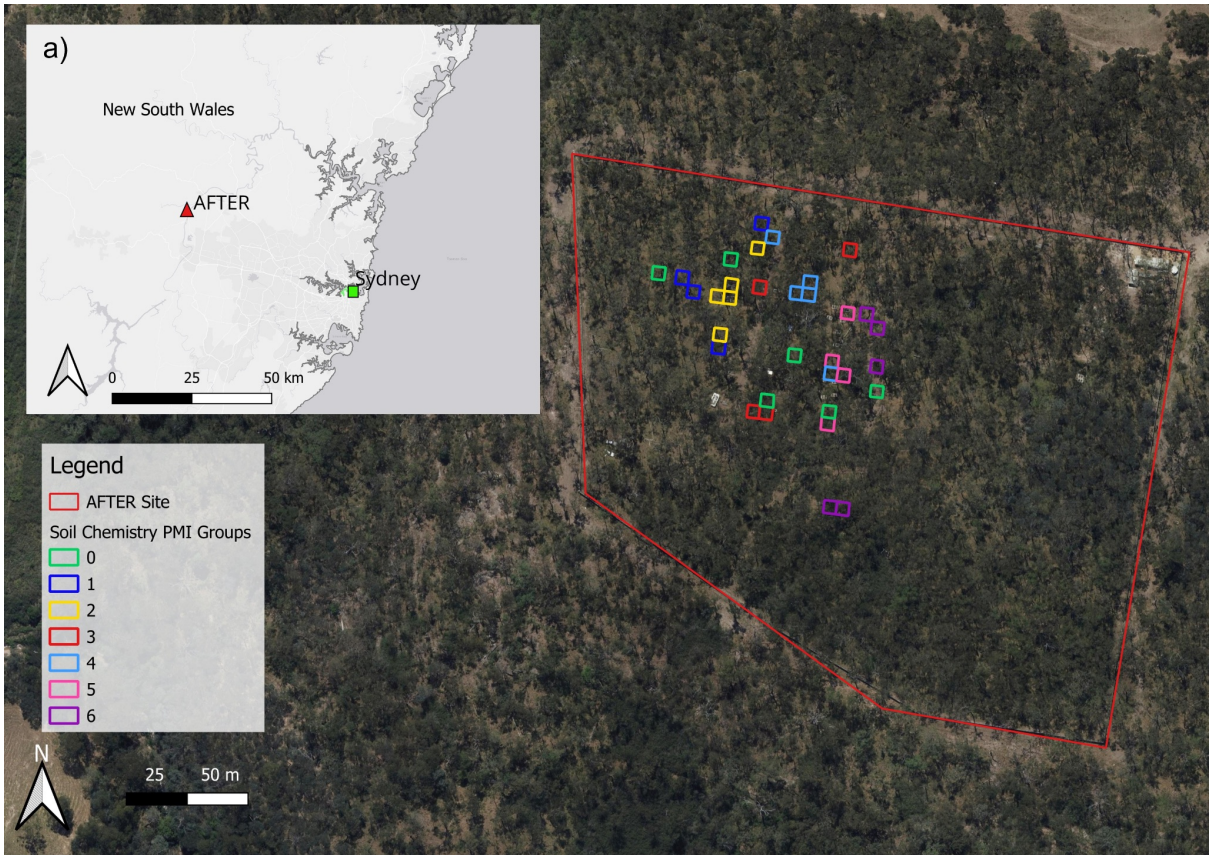

Figure 1. The AFTER facility and sampling locations. The AFTER site is divided into plot areas of 3m x 3m. The facility boundary (red line) and sampled plots are outlined. Inset indicates the location of AFTER within the Sydney basin, New South Wales. Satellite imagery source: QGIS v 3.24.3.

2.2 Sampling

The AFTER facility utilises an organised plot approach of 3 x 3m^2 in dimension with 50 potential plot locations. At the time of this study a total of 33 plots were sampled with 27 of those having human donors (8 female, 19 males; 69.9 - 93.9 kg) placed supine on the soil surface between 2016 and 2025 and the remaining plots were treated as control sites. The 27 plots were randomly selected having divided the site into age cohorts (Table 1). Four of the donors were clothed (cohorts 1-3) at the time of placement with the remaining 23 unclothed. Structured wire cages (1m x 1m x 2m) were used to cover donors and deter scavenging and disturbance while promoting access to insect and climate variables.

Table 1. Summary of the division of 33 individual plots by postmortem interval (PMI) and the degree of decomposition of human remains in each cohort.

Cohort	N	PMI (years)	Clothing (n)	Decomposition stage
0	6	0 (Control)	-	-
1	5	< 1	1	Advanced
2	7	1-2	2	Dry Remains
3	4	4-5	1	Skeletonised
4	3	7	-	Skeletonised
5	4	8	-	Skeletonised
6	6	9	-	Skeletonised

A composite sampling approach was implemented around existing surficial remains where four individual samples from each plot were collected at 0-10 cm depth intervals from the head and groin regions and upper limbs (~50 g per spot) homogenised and subsampled for chemical and biological analysis. A non-composite sample was taken from 3 of the plots to establish the representativeness of the composite sampling approach. Details of these additional samples are located in Supplemental files (S3, S7 and S11). Samples were collected using sterilised stainless-steel push corer and spatulas, with samples placed in sterile plastic Falcon tubes (16s RNA) or plastic ziploc bags (chemical analysis), and stored on ice in the field (for less than five hours) before being stored at -80°C. The corer was thoroughly cleaned between samples with deionised water followed by ethanol.

Soil samples were analysed by a NATA-accredited facility, using standard methods compliant with ISO/IEC 17025. The analytical approaches from Rayment & Lyons (2011) were applied for pH (4A1), electrical conductivity (3A1), plant-available phosphorus (Bray 1 9E2, Colwell 9B2), exchangeable cations (Ca, Mg, K, Na: 15D3; exchangeable H: 15G1), DTPA-extractable micronutrients (Zn, Mn, Fe, Cu: 12A1) and $CaCl_2$-extractable boron (12C2). Total carbon, total nitrogen, estimated organic matter, and C:N ratio were quantified using LECO. Soluble cations and soluble P were determined using Morgan 1, while Bray 2 phosphorus was analysed using a modified approach. KCl-extractable nitrate-N, ammonium-N, and sulfur were measured using Inhouse S37, and $CaCl_2$-extractable silicon was determined using Inhouse S11. Total metals and metalloids Ag, Al, As, Ca, Cd, Co, Cr, Cu, Fe, Hg, K, Mg, Mn, Mo, Na, Ni, Pb, P, S, Se, Si, Zn) were determined following 1:3 nitric:HCl digestion using APHA 3125 (ICP-MS) or APHA 3120 (ICP-OES) as specified for each element. Maximum soil chloride concentration was estimated using the laboratory standard calculation (EC × 640). Values below detection limits were reported as half of the detection limit.

2.3 DNA extraction, 16S rDNA gene PCR amplification, and amplicon sequencing

DNA extractions were conducted on subsampled soil (300 mg) in triplicate using the DNeasy PowerSoil Pro Kit (Qiagen) according to the manufacturer's quick-start protocol, with the following additional steps to improve yield: samples were incubated at 65°C for 10 minutes in a water bath and at 95°C in a heat block for 10 minutes (Cobaugh et al., 2015). Glass beads (0.1mm) were added to tubes prior to samples undergoing two beating steps of 30 seconds at

medium speed with a 1 minute rest in between. Triplicate sample DNA was pooled at the final step to improve yield. The remaining protocol was unchanged.

DNA yield was assessed using a DeNovix DS-11+ spectrophotometer (File S3). Samples were PCR amplified and sequenced at the Ramaciotti Centre for Genomics (UNSW Sydney, Australia) on the Illumina MiSeq platform. PCR amplification was performed using the 515F and 806R amplicon primer set to target the V4 region of the 16S rDNA gene, followed by attachment of unique tags for Illumina sequencing in the second PCR to generate the final amplicons (2 × 250bp pair-end reads). This was in line with previous protocols outlined in Bolyen et al., (2018), and the library prepared as previously described (Illumina, 2016). 16S rDNA amplicon sequencing reads were processed using the QIIME2 platform (Version 2024.2; Bolyen et al., 2018). Quality control was conducted by truncating sequences at 245bp to remove low-quality regions (<Q25) and the first 10bp of reads to ensure primer and adaptor removal. Amplicon Sequence Variants (ASVs) were determined using DADA2 denoising (Callahan et al., 2016) with QIIME2, which merged paired reads and removed chimeric sequences. Taxonomy was assigned to representatives of each ASV using the QIIME2 Feature Classifier (Bokulich et al., 2018) and the SILVA Database (V138; Robeson et al., 2020) to the genus level (level six) in line with the ontology of the library database, with 'unidentified' representing a discrete group of an unknown genus, and the mean is presented for duplicated samples. Data was rarefied to 45,000 before statistical analysis based on mean observed features (File S4) to eliminate the effect of uneven sampling depth (Cobaugh et al., 2015; Emmons et al., 2020; Procopio et al., 2019).

Statistical analysis

Distributional differences between treatment cohorts were visualised using cohort-wise boxplots with medians, interquartile ranges, and dispersion for every analyte. A Pearson correlation analysis was used to quantify linear relationships among all soil chemical variables, visualised as a correlation matrix heatmap to identify clusters of positively and negatively associated parameters (File S1). Multivariate statistics and diversity analyses were conducted within QIIME2 as follows. Bray-Curtis similarity was calculated between each sample and visualised as a Principle Coordinates Analysis (PCoA) using Emperer (Vázquez-Baeza et al., 2013). The significance of clustering between each grouping was determined using ANOSIM with 999 permutations (Anderson, 2001). Differences in alpha-diversity (ASV richness, Shannon Index, and Pielou evenness) were assessed in QIIME2 and were calculated using a Kruskal-Wallis test. The relationship between environmental variables (including Bray 1, Colwell-P, pH, DTPA-Zn, Total nitrogen and phosphorus) and microbial community diversity (beta diversity) was determined using BIOENV (Clarke & Ainsworth, 1993) and redundancy analysis (Mieczan et al., 2022) in R software (Version 4.4.0; R Core Team 2021).

3. Results and Discussion

3.1 AFTER soil physical and chemical properties

Soil pH was 5.13 ± 0.20 in the control cohort and increased to 6.08 ± 0.49 in the year 1 cohort (Figure 2). In later cohorts pH remained close to, or slightly above, the control with a return towards the control pH (5.52 ± 0.18 at 1–2 years; 5.21 ± 0.08 at 4.5–5 years; 5.18 ± 0.18 in the mixed 1–7.5 year cohort; 5.00 ± 0.18 at 8 years; 5.30 ± 0.12 at 8.5–9 years). Electrical conductivity (EC) was 0.05 ± 0.01 dS m^{-1} in controls, and followed a similar pattern with increased values of 0.45 ± 0.35 dS m^{-1} at 0.25–0.5 years, and then a decline toward control values in older cohorts (0.09 ± 0.02 dS m^{-1} at 1–2 years; 0.07 ± 0.02 dS m^{-1} at 4.5–5 years; 0.08 ± 0.03 dS m^{-1} in the mixed 1–7.5 year cohort; 0.05 ± 0.01 dS m^{-1} at 8 years; 0.04 ± 0.01

dS m^{-1} at 8.5–9 years). There were no significant differences in within-group variability among cohorts ($F = 0.87$, $p = 0.53$), indicating that the observed multivariate shifts were due to differences in group means rather than unequal variances.

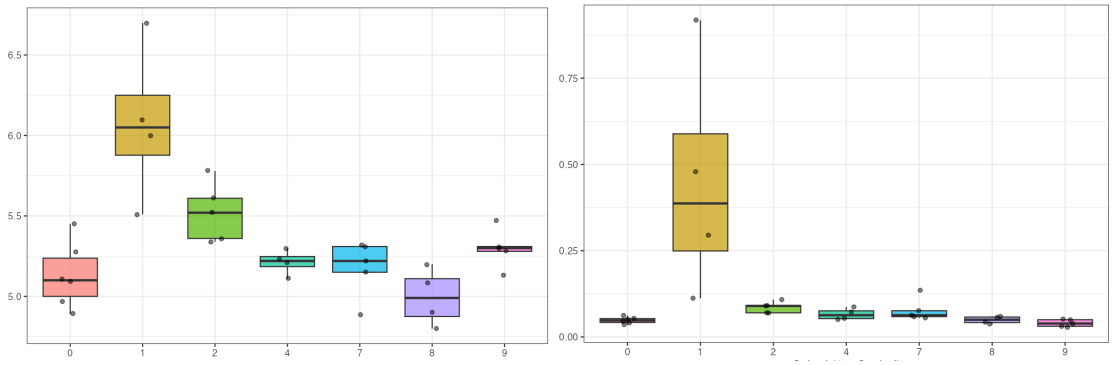

Figure 2. Soil pH and EC (dS m) from 0 (baseline) to 9 years PMI

The soil pH has positive correlation to soil exchangeable ions (File S1). Exchangeable calcium was 1.50 ± 0.41 cmol(+)/kg in the control cohort and increased in all treated cohorts, reaching 1.95 ± 1.25 cmol(+)/kg in the year 1 cohort (Figure 3). In older cohorts, exchangeable calcium remained elevated but variable, spanning 0.94–1.92 cmol(+)/kg across sites. Exchangeable magnesium was 1.24 ± 0.25 cmol(+)/kg in controls, increased to 1.62 ± 0.68 cmol(+)/kg, and remained above or comparable to controls in all later cohorts (0.95–1.44 cmol(+)/kg). Exchangeable potassium averaged 0.24 ± 0.04 cmol(+)/kg in controls, rose sharply to 1.00 ± 0.24 cmol(+)/kg in the earliest postmortem cohort, and then declined but stayed above control levels (0.28–0.56 cmol(+)/kg) in subsequent years. Exchangeable sodium was 0.14 ± 0.03 cmol(+)/kg in controls, peaked at 1.34 ± 0.84 cmol(+)/kg at within the 1 year cohort, and then decreased toward background values in older cohorts (0.11–0.52 cmol(+)/kg). Exchangeable aluminium was 1.79 ± 0.61 cmol(+)/kg in controls but declined markedly in the earliest cohort (0.28 ± 0.03 cmol(+)/kg) and remained lower in all treated groups (0.28–2.05 cmol(+)/kg, depending on PMI stage). Exchangeable hydrogen was 0.90 ± 0.40 cmol(+)/kg in controls, decreased to 0.72 ± 0.60 cmol(+)/kg, and remained at or above these reduced levels across older cohorts (0.72–1.53 cmol(+)/kg). Total calcium and magnesium displayed substantial cohort-level variability. Calcium was 516.0 ± 118.7 mg/kg in controls, increased to 748.8 ± 317.0 mg/kg at 0.25–0.5 years, and reached its highest levels in the mixed 1–7.5 year group (828.4 ± 396.5 mg/kg). Magnesium was 325.0 ± 46.4 mg/kg in controls and fluctuated between 241.2–405.6 mg/kg across the burial cohorts, with its highest values also occurring in mid-stage soils.

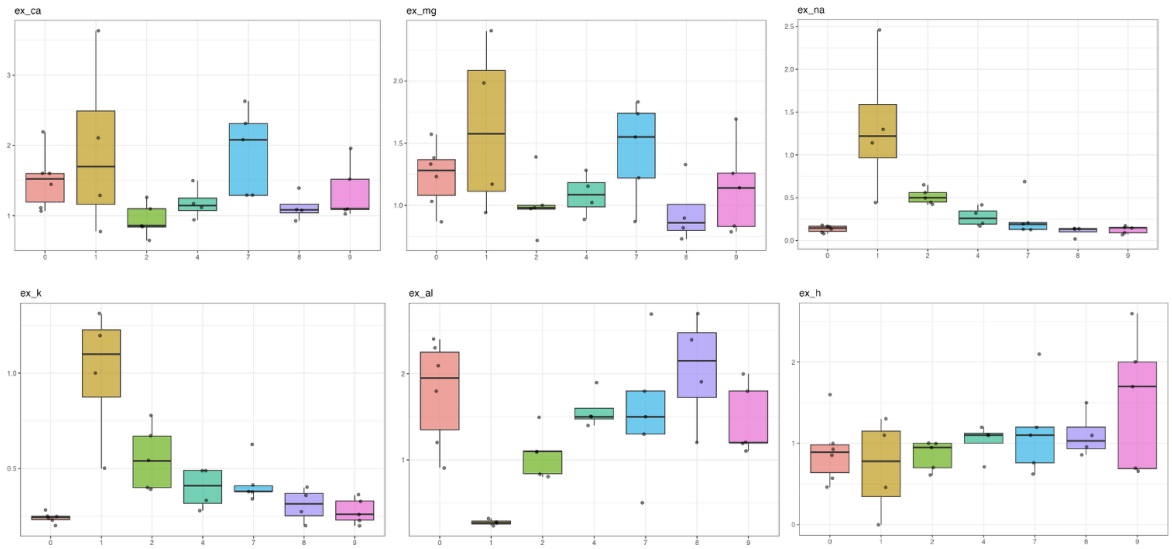

Figure 3. Soil exchangeable ions from 0 (baseline) to 9 years PMI. Values in cmol(+)/kg.

Total nitrogen was 0.26 ± 0.03% in controls and increased substantially in the earliest postmortem cohort (0.57 ± 0.16%) (Figure 4). Although total nitrogen declined thereafter, it remained above or comparable to baseline across all older cohorts (0.24–0.41%). Nitrate-N was 1.03 ± 0.51 mg/kg in controls, increased sharply to 2.28 ± 1.14 mg/kg at 1 year, and then declined but stayed above or near baseline levels in most later cohorts (0.70–1.38 mg/kg). Ammonium-N averaged 12.72 ± 0.86 mg/kg in baseline, increased to 598.75 ± 463.64 mg/kg at 0.25–0.5 years, and then decreased to levels well below the early peak and within the range of background values in older cohorts (5.70–21.12 mg/kg). Bray-1 P was 2.45 ± 0.95 mg/kg in controls, increased to 52.5 ± 46.7 mg/kg in the earliest cohort, and remained elevated relative to controls in all older cohorts (4.9–13.2 mg/kg). Bray-2 P, Colwell P, and soluble P followed the same pattern, showing a pronounced increase in the earliest postmortem soils and persisting at levels higher than controls across all subsequent cohorts. Total phosphorus showed the strongest early enrichment, rising from 135.6 ± 45.7 mg/kg in controls to 439.8 ± 142.2 mg/kg, and although declining thereafter, it remained above background at all later stages (185.2–284.8 mg/kg). Total sulfur followed this pattern, increasing from 176.3 ± 21.8 mg/kg in controls to 446.0 ± 111.1 mg/kg in the early cohort, with sustained enrichment in older soils (222.8–352.8 mg/kg). Nutrients behaved independently, with no significant linear relationships among any of the nitrogen species, phosphorus fractions, or sulfur measures (File S1).

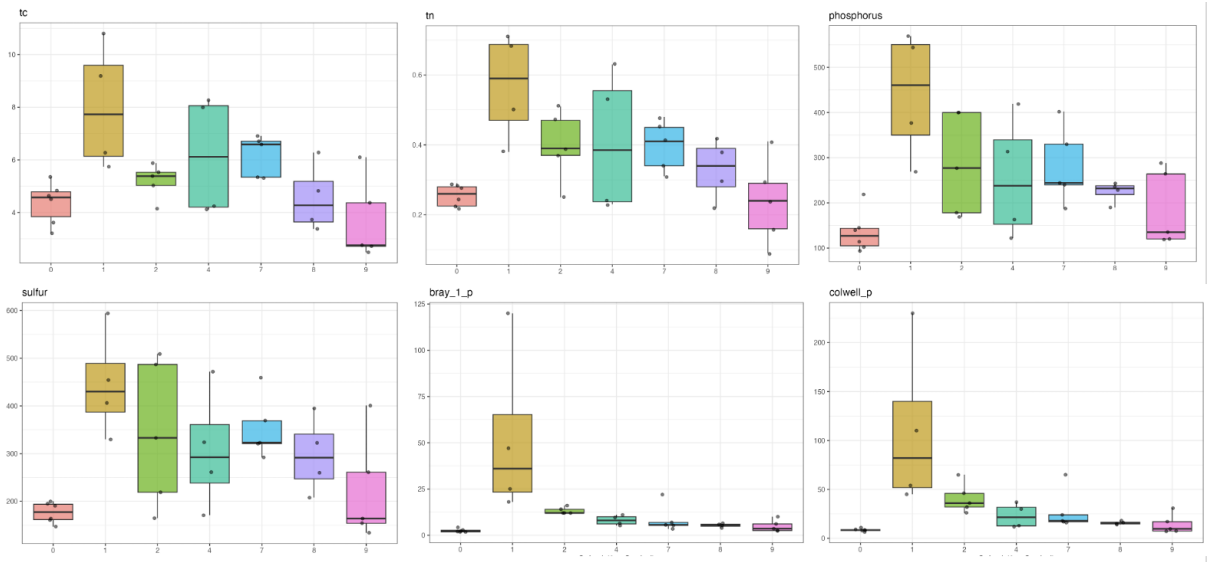

Figure 4. Total carbon, nitrogen and phosphorus and Bray 1 and Colwell P extractions.

Bioavailable metals displayed a clear trend through the PMI cohorts (Figure 5). DTPA-Zn averaged 17.20 ± 32.28 mg/kg in controls, remained comparable in the earliest PMI cohort (14.10 ± 6.75 mg/kg), and then increased sharply in older soils, reaching substantially elevated concentrations (71.72–111.50 mg/kg) across mid- to late-stage cohorts. DTPA-Cu was 0.25 ± 0.05 mg/kg in controls, increased modestly at 0.25–0.5 years (0.38 ± 0.15 mg/kg), and remained at or below control levels in later cohorts (0.07–0.32 mg/kg) with substantial variability. DTPA-Mn was 22.72 ± 5.92 mg/kg in controls, increased to 39.98 ± 12.26 mg/kg in the earliest cohort, and then declined but generally remained near or above background levels in older cohorts (8.40–16.74 mg/kg). DTPA-Fe was 166 ± 33 mg/kg in controls, rose to 307 ± 67 mg/kg in the earliest cohort, and remained consistently elevated across all older cohorts (215–316 mg/kg). Arsenic, cadmium, lead, nickel, cobalt, selenium, and molybdenum occurred at low concentrations in all cohorts, with many measurements close to detection limits.

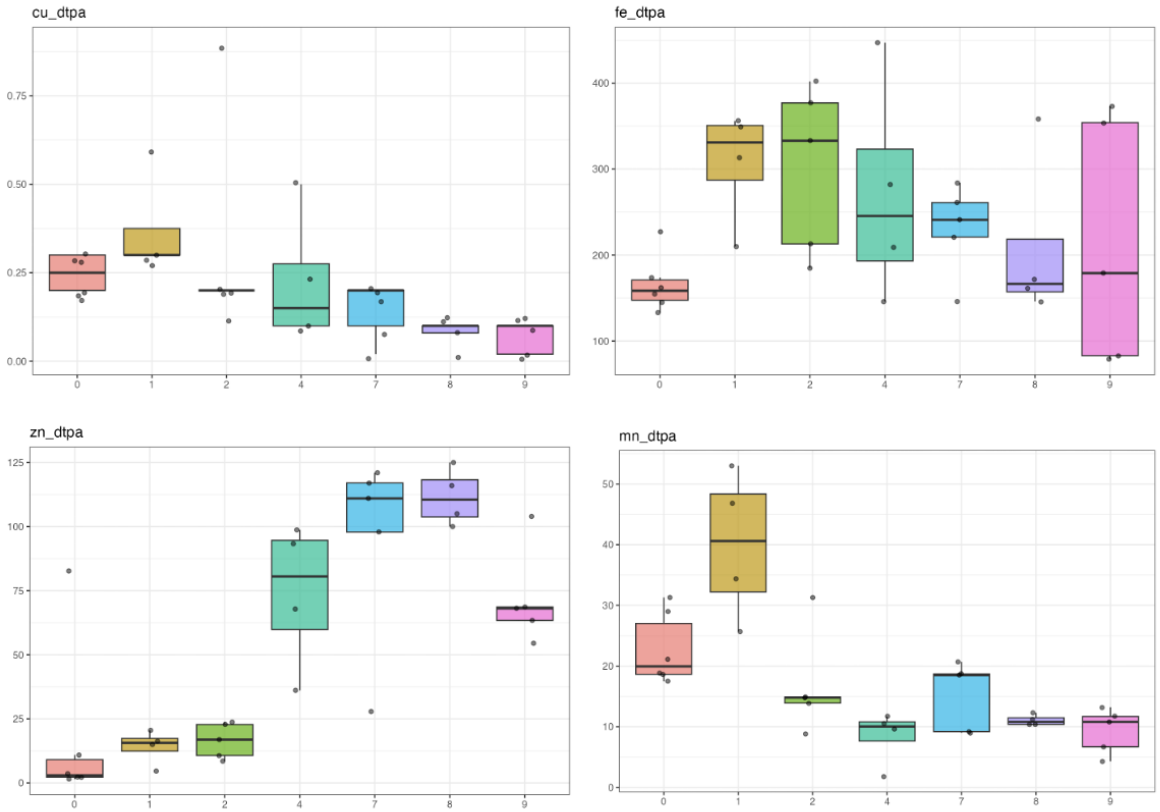

Figure 5. Soil exchangeable ions from 0 (baseline) to 9 years PMI. Values in mg/kg.

Among total metals, iron increased from 8236.7 ± 2375.9 mg/kg in controls to 8887.5 ± 4767.5 mg/kg within the first year cohort and then reached very high concentrations in older cohorts (14,047.5–20,050.0 mg/kg) (Figure 6). Zinc increased from 27.1 ± 37.4 mg/kg in controls to in early cohorts (25.3–31.6 mg/kg), followed by large increases in mid- to late-stage cohorts (146.5–224.3 mg/kg). Arsenic increased from 1.21 ± 1.34 mg/kg in controls to 2.47–4.26 mg/kg in the 4.5–9 year cohorts. Molybdenum increased from 0.18 ± 0.20 mg/kg in controls to 0.32–0.46 mg/kg in cohorts 3–6. Cadmium was below detection limits in controls but reached 1.53 ± 1.07 mg/kg at 1 year before declining to ≤0.60 mg/kg in older cohorts. Nickel, lead, chromium, and cobalt varied within relatively narrow ranges around control values, with silver, mercury and boron at below detection limits.

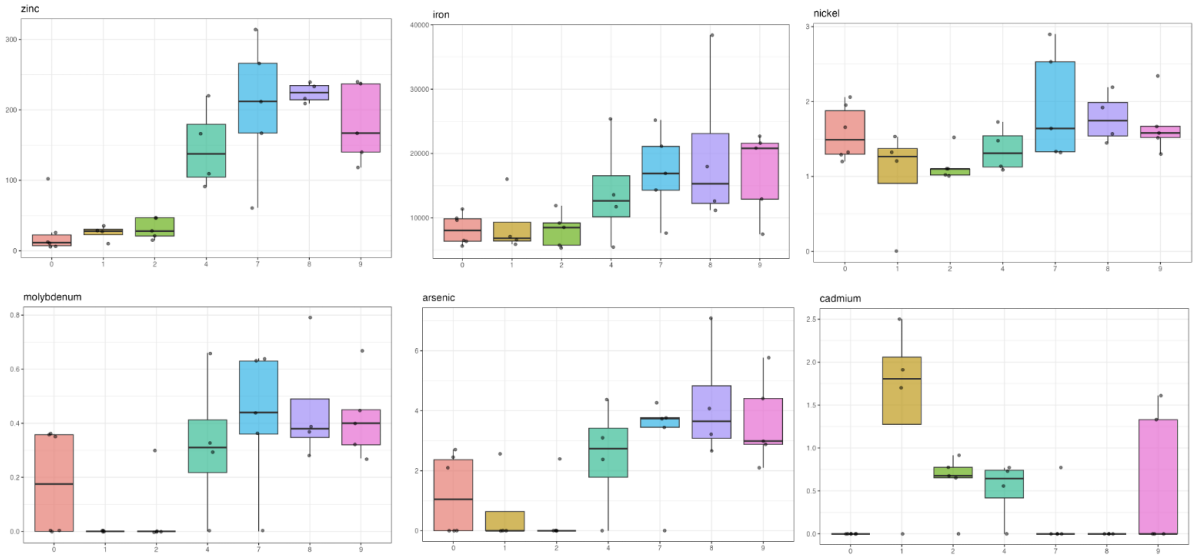

Figure 6. Soil exchangeable ions from 0 (baseline) to 9 years PMI. Values in mg/kg.

3.2 Microbial community and physiochemical controls

The mean number of sequence reads for the 16S rDNA per sample was 66,418, ranging from 2 to 45,053 (File S4). Only one sample (A_19_02, cohort 1) was eliminated from further analyses due to a low read of 2. Denoising resulted in 52,916 ASVs with an average of 1470 per sample. Alpha diversity for the microbial community was significantly lower in cohorts with the earliest PMI (1 and 2) and therefore, most decomposition activity, for observed features (p=0.004, H=19.38; File S5) and Shannon Index (p=0.001, 24.08; File S6) relative to control (0) and extended PMI cohorts (3-6) at AFTER. Mean and range of diversity was similar between the control cohort and cohorts with extended PMI's (3-6) (Figure 7). The Pielou evenness also supports that single taxa did not dominate with means between 0.80-0.88 across all PMI cohorts (File S7). This is in line with findings from Mason et al., (2022), where alpha diversity of soil bacterial communities is high in control groups, and decreases with the introduction of decomposition fluids.

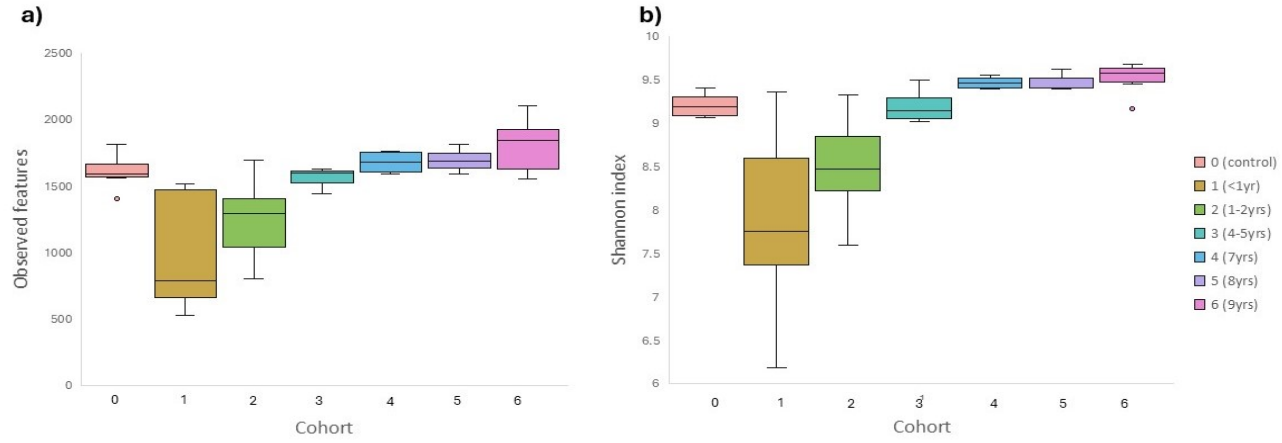

Figure 7. Alpha diversity of the microbial community at AFTER (n=35 samples, 7 cohorts) for a). observed features, and b). Shannon Index for the PMI cohorts.

Analysis of beta diversity using PCoA (Bray-Curtis dissimilarity) showed a clear difference in the microbial community by postmortem interval. Control (cohort 0) and the oldest PMI cohort (cohort 6, 9 years postmortem) have high similarity, followed by the cohorts with PMI ranging

4-8 years (cohort 4-5). The largest difference was observed for the earliest postmortem cohorts (cohort 1-2) relative to all others (Figure 8). ANOSIM results showed that the postmortem interval was the main factor driving changes between the early postmortem cohorts (0.5-2 years) and all other samples (p=0.001, strength = 0.39).

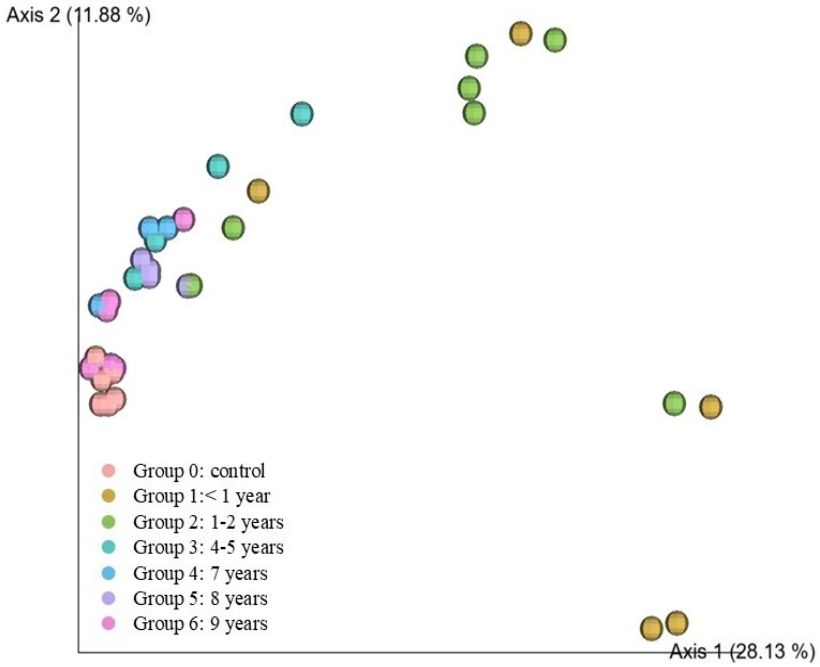

Figure 8. Beta diversity ordination of the microbial community composition from AFTER surface plots (n=35 samples, 7 cohorts) by postmortem interval as a proxy for time (unconstrained principal coordinate analysis (PCoA) using Bray-Curtis dissimilarity).

The BIOENV analysis showed that the dominant driver of the microbial community was Colwell-P) (correlation = 0.70). The highest combination of variables was Bray-1-P, Colwell-P, Ammonium-N, pH and P (correlation = 0.65) (Table 3). Patterns in beta diversity are best explained by these variables, reflecting the impact of the introduction of decomposition fluid on the soil microbial community, particularly during active stages of decomposition. This is supported by the redundancy analysis, which showed early shifts in phosphorus, nitrogen, and carbon load to the soil along with increasing pH, DTPA-Fe and exchangeable-Na correlate to cohort groups 1-3 (Figure 9). Cohort 4 appears transitional and is partially explained with the parameters from cohort groups 1-3 along with parameters DTPA-Zn, Ca:Mg ratio, and acidity measures exchangeable-H and exchangeable-Al. The older cohort 6 is correlated to these same parameters but shows a progression back to the control cohort 0 signifying a potential return to the original soil conditions.

Table 3. BIOENV analysis correlation values for microbial community and physiochemical properties for AFTER soil plots. Variables included were Phosphorus (P), pH, total nitrogen (TN), DTPA-extractable zinc (DTPA-Zn) and postmortem interval (PMI).

Variables	Size	Correlation
Colwell-P	1	0.7
Bray-1-P, Colwell-P	2	0.7
Bray-1-P, Colwell-P, Ammo	3	0.7
Bray-1-P, Colwell-P, Ammonium-N, Phosphorus	4	0.69
Bray-1-P, Colwell-P, Ammonium-N, pH, Phosphorus	5	0.66
Bray-1-P, Colwell-P, Ammonium-N, pH, TN, Phosphorus	6	0.65
Bray-1-P, Colwell-P, Ammonium-N, pH, Zn-DTPA, TN, Phosphorus	7	0.63
Bray-1-P, Colwell-P, Nitrate-N Ammonium-N, pH, Zn-DTPA, TN, Phosphorus	8	0.63
Bray-1-P, Colwell-P, Nitrate-N Ammonium-N, pH, Zn-DTPA, TC, TN, Phosphorus	9	0.61

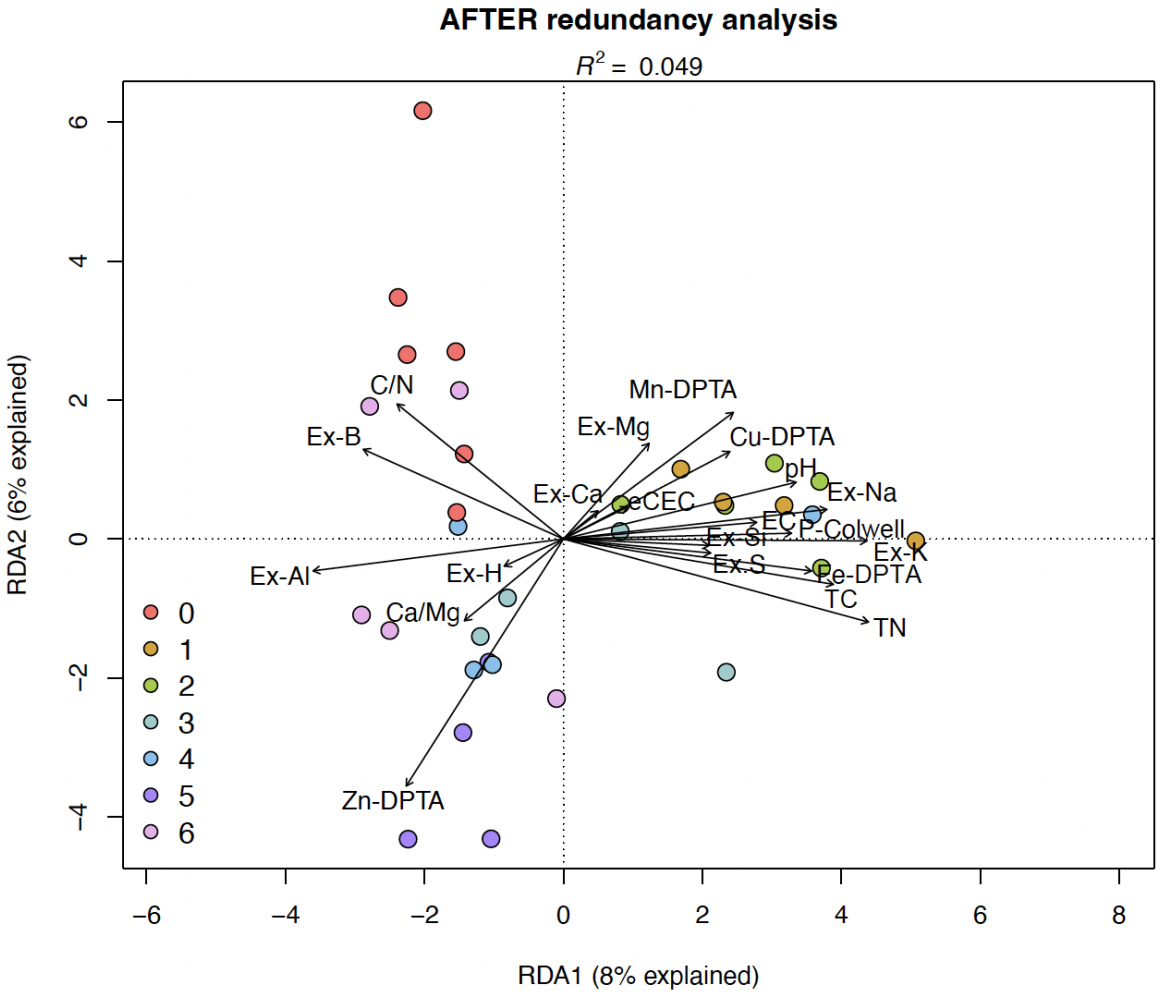

Figure 9. Redundancy analysis for microbial community and physiochemical properties for AFTER cohorts.

The 16S rDNA gene amplicon sequences showed that at the phylum level, Pseudomonadota and Actinomycetota were most prevalent overall across all sampled plots at the AFTER site (Figure10). Acidobacteriodota, Verrucomicriobiota and Planctomycetota were more prevalent in control (0) and older PMI cohorts (3-6) compared to early PMI cohorts (1-2), while Bacillota and Bacteriodota exhibited greater abundance in early PMI cohorts. Microbial community composition varied with postmortem interval (as shown by the ANOSIM findings). The observed taxa were similar to those found in previous decomposition studies conducted internationally (Mason et al., 2022; Taylor et al., 2024). The greatest microbial diversity of soil occurred in the control cohort, with diversity decreasing in early PMI cohorts before increasing to ward control levels from 4.5 years postmortem (cohort 3) onwards. This aligns with prior human decomposition research (Mason et al., 2022; Taylor et al., 2024). Based on the BIOENV and redundancy analysis, nutrient loading in the first 3 years are a key factor driving patterns in the soil microbial community.

At the class level Alphaproteobacteria (p. Pseudomonadota) was abundant in the control cohort (median 26.15%) declining during the first 6 months of decomposition (cohort 1; 18.13%) and increasing once decomposition progressed to advanced and dry stages (cohort 2-6). This copiotrophic bacteria has been identified previously as being prevalent in late stages of

decomposition (Cobaugh et al., 2015), possibly due to this taxa using more chemically complex products of decomposition, as well as exhibiting a negative correlation with pH (Zhou et al., 2024). Terriglobia (p. Acidobacteria; median 10.84%) followed a similar pattern to Alphaproteobacteria. Terriglobia is not commonly reported in human decomposition studies. However, the decrease in Acidobacteria during active decomposition has been described in previous studies (Mason et al., 2024; Metcalf et al., 2013), attributed to the oligotrophic characteristics in response to a pulse of nutrients into the soil. The increase in abundance of Pseudomonadota and Acidobacteria in the soil from active decomposition to the dry remains stage has been described (Damann et al., 2015; Deel et al., 2021), suggesting that these taxa may be useful in estimation of of PMI in in dry and skeletonised remains. The Bacterial classes Verrucomicrobiae (median 16.09%) and Planctomycetia (median 9.56%), were also prevalent in the control cohort, decreasing in samples from early PMI plots (cohort 1) before a gradual return to control levels. Verrucomicrobiota, a prevalent taxa in soil on the east and southeast Australian coast, is an oligotroph, thriving in low pH environments. Decreases in the prevalence of this bacteria during active stages of decomposition has been reported previously (Singh et al., 2018), associated with increases in nutrient availability (Taylor et al., 2024). Planctomycetia, also oligotrophic, exhibited the greatest abundance in control plots compared to a marked decrease in early PMI groups, which can be attributed to this taxa likely being outcompeted when decomposition fluid seeps into the soil by fast-growing organisms (such as Gammaproteobacteria) that can respond to the influx of new nutrients (Cobaugh et al., 2015).

Bacterial classes Gammaproteobacteria (median 24.09%), Actinomycetes (median 23.36%), Clostridia (median 8.14%) and Bacteroidia (median 6.0%) were observed as the most abundant taxa in early PMI plots (cohort 1) when decomposition is most active, with abundance decreasing towards control levels between 1 year (Group 2) and 9 years postmortem. The increase in abundance of Gammaproteobacteria and Clostridia is supported by previous studies (Cobaugh et al., 2015; Metcalf et al., 2013). These taxa have been identified as dominant taxa in decomposition fluid (Mason et al., 2022), the likely source of the soil communities during active decomposition. Abundance of Actinomycetes followed a similar pattern to Gammaproteobacteria. Actinomycetes is known in soil studies for its role in nitrogen fixation and organic matter decomposition with a preference for neutral pH (6-8) and low moisture soils (Nazari et al., 2022). This class of bacteria is under-reported in human decomposition studies, but at the phylum level, Actinomycetota is known to be highly enriched directly under decomposing remains with a PMI of 6 months (Fouché et al, 2024), which aligns with the findings of the current study. Similarly, the class Bacteroidia is not typically reported in human decomposition studies. At the phylum level, Bacteroidota is a common anaerobic human gut bacteria that peaks in the body during active decay (ie. Group 1) and is detected in soil with the presence of a cadaver (Singh et al., 2018). Singh et al (2018) also suggest this phylum blooms in soil in advanced stages of decomposition (Groups 2-9) and can be a marker of extended PMI, however, this was not observed in the present study. Instead, our findings align with Procopio et al (2019), who found Bacteroidota peaked at 4 months postmortem before decreasing progressively towards control levels after 6 months.

.

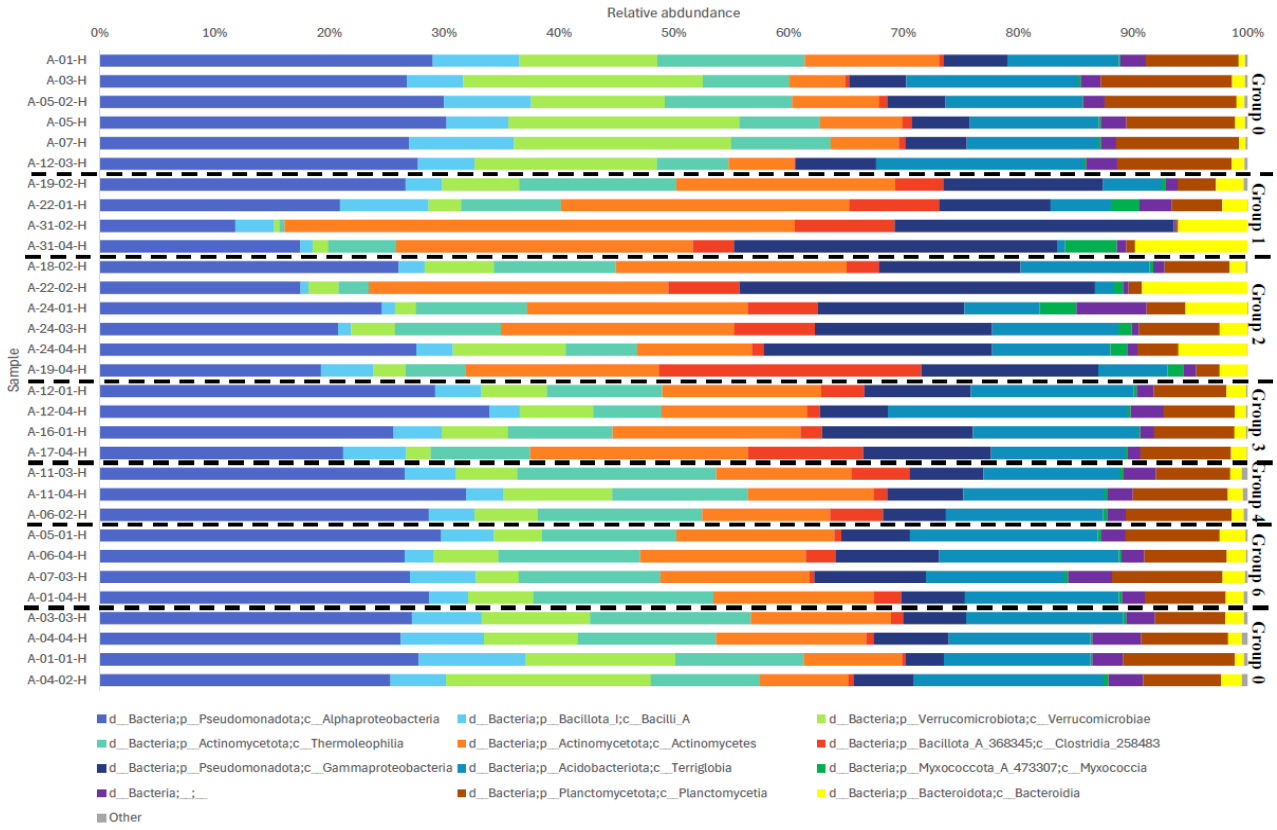

Figure 10. Microbial community composition relative abundance for AFTER soil plots resolved at class level. Soil plots are arranged by cohort (0 – 6) according to PMI (Table 1). Taxa that contribute <1% are classified as Other.

3.3 Implications for postmortem interval estimation for extended time periods

The results of the microbial analysis overall indicate statistically significant increases and decreases in abundance of several taxa at defining stages of decomposition. The observations presented here exhibit similarities to previous studies, despite methodological differences such as geographic location (Mason et al., 2022; Singh et al., 2018) and cadaveric species (Cobaugh et al., 2015; Metcalf et al., 2013; Procopio et al., 2019), and support the concept of a microbial clock for reliable PMI estimation during the first six months to a year. However, observed differences, including an absence of the bacterial classes Actinomycetes and Bacteroidia in earlier studies, suggest that shifts in microbial diversity and abundance may be region or climate specific (Carter et al., 2015). The redundancy analysis indicates that early cohorts cluster with strong nutrient and trace element signals characteristic of active decomposition, with microbial communities aligning with parameters such as the carbon to nitrogen ratio, exchangeable-B, exchangeable-Ca, exchangeable-Mg, exchangeable-H, and DPTA-Zn. This pattern is consistent with the nutrient driven restructuring of soil microbiota during the first few years after death as decomposition derived carbon and nitrogen stimulate substantial changes in community composition. As nutrient availability declines, the influence of nutrient enriched soil chemistry weakens and taxa that respond to these early inputs decrease in abundance. Despite this decline, the ordination shows that older cohorts retain a modest but detectable chemical signature characterised by variables associated with slower soil processes, including pH, electrical conductivity, cation exchange capacity, Colwell phosphorus, exchangeable Na, and residual metal fractions such as DPTA-Cu and DPTA-Mn. By approximately eight years, samples converge near the origin of the ordination space, indicating broad recovery of both soil chemistry and microbial communities toward baseline conditions.

This trajectory suggests that microbial and nutrient based indicators are most informative during the first few years, while longer term PMI estimation increasingly relies on more persistent geochemical markers preserved in the soil.

4. Conclusions

These findings demonstrate that human decomposition leaves a measurable but time-limited imprint on soil chemistry and microbial diversity, defined by strong nutrient and taxonomic responses in the year and progressively weaker signals thereafter. Early decomposition produces marked shifts in microbial diversity, elevated nutrient pools and sustained increases in trace elements that shape community composition, with responsive taxa aligning closely with enriched soil chemistry. As nutrients dissipate and microbial assemblages return toward pre-decomposition states, the soil retains only a modest chemical signature characterised by slower-changing variables and select trace metals, with both microbial and chemical profiles converging toward baseline by approximately eight years. Overall, this study confirms that soil communities and geochemical indicators provide robust PMI information during early and mid-stage decomposition and that longer-term interval estimation depends increasingly on persistent chemical markers that endure beyond the period of active nutrient release.

Data availability statement

16S rDNA gene sequences are available from the National Centre for Biotechnology Information (NCBI) under the project accession number PRJNA1372398.

Funding

This research was supported by in-kind contributions from the Australian Facility for Taphonomic Experimental Research (AFTER).

Conflict of interest disclosure

The authors declare no competing interests.

Acknowledgements

We acknowledge the assistance from the University of Technology of Sydney and Western Sydney University. We thank Mark Emanuel for contributions to sample preparation. All ethical and legal requirements associated with researching donated human cadavers were acquired through the University of Technology Sydney (UTS) Human Research Ethics Committee (HREC ETH18-2999/ WSU H13403) and the UTS Body Donation Program with consent provided by donors in accordance with the New South Wales (NSW) Anatomy Act (1977). We are indebted to all the donors involved in research at AFTER and to the invaluable contribution they have made to forensic science.

References

Aitkenhead-Peterson, J. A., Owings, C. G., Alexander, M. B., Larison, N., & Bytheway, J. A. (2012). Mapping the lateral extent of human cadaver decomposition with soil chemistry. *Forensic Science International, 216*(1–3), 127–134. https://doi.org/10.1016/j.forsciint.2011.09.007

Carter, D. O., Yellowlees, D., & Tibbett, M. (2007). Cadaver decomposition in terrestrial ecosystems. *Naturwissenschaften, 94*(1), 12–24. https://doi.org/10.1007/s00114-006-0159-1

Cobaugh, K. L., Schaeffer, S. M., & DeBruyn, J. M. (2015). Functional and structural succession of soil microbial communities below decomposing human cadavers. *PLOS ONE, 10*(11), e0130201. https://doi.org/10.1371/journal.pone.0130201

Damann, F. E., Williams, D. E. & Layton, A. C. (2015). Potential use of bacterial community succession in decaying human bone for estimating postmortem interval. *Journal of forensic sciences* 60, 844–850. https://doi.org/10.1111/1556-4029.12744

Deel, H., Emmons, A. L., Kiely, J., Damann, F. E., Carter, D. O., Lynne, A., Knight, R., Xu, Z. Z., Bucheli, S., & Metcalf J. L. (2021). A Pilot Study of Microbial Succession in Human Rib Skeletal Remains during Terrestrial Decomposition. *mSphere*, 6(4). https://doi.org/10.1128/mSphere.00455-21

Emmons, A. L., Mundorff, A. Z., Keenan, S. W., Davoren, J., Andronowski, J., Carter, D. O., & DeBruyn, J. M. (2020) Characterizing the postmortem human bone microbiome from surface-decomposed remains. PLoS ONE 15(7): e0218636. https://doi.org/10.1371/journal.pone.0218636

Guo, Y., Fu, X., Liao, H., Hu, Z., Long, L., Yan, W., & Ding, Y. (2016). Potential use of bacterial community succession for estimating post-mortem interval as revealed by high-throughput sequencing. *Scientific Reports, 6*, 24197. https://doi.org/10.1038/srep24197

Illumina. (2016). *Nextera ® DNA Library Prep Reference Guide*. Retrieved December 13 2025, from https://support.illumina.com/content/dam/illumina-support/documents/documentation/chemistry_documentation/samplepreps_nextera/nexteradna/nextera-dna-library-prep-reference-guide-15027987-01.pdf

Isbell, R. F., National Committee on Soil and Terrain (NCST), & Commonwealth Scientific and Industrial Research Organisation (CSIRO) Publishing. (2021). *The Australian Soil Classification*, *third ed*. CSIRO Publishing, Victoria.

Jaggers, R., Rogers, T. L., & Robertson, J. M. (2009). The effects of soil environment on postmortem interval: A macroscopic analysis. *Journal of Forensic Sciences, 54*(3), 605–610. https://doi.org/10.1111/j.1556-4029.2009.01160.x

Mason, A. R., McKee-Zech, H. S., Hoeland, K. M., Davis, M. C., Campagna, S. R., Steadman, D. W., & DeBruyn, J. M. (2022). Body Mass Index (BMI) Impacts Soil Chemical and Microbial Response to Human Decomposition. *mSphere*, 26, e0032522. https://doi.org/10.1128/msphere.00325-22

Mason, A. R., McKee-Zech, H. S., Steadman, D. W., & DeBruyn, J. M. (2024). Environmental predictors impact microbial-based postmortem interval (PMI) estimation models within human decomposition soils. *PLOS ONE, 19*(1), e0311906. https://doi.org/10.1371/journal.pone.0311906

Metcalf, J. L., Wegener Parfrey, L., Gonzalez, A., Lauber, C. L., Knights, D., Ackermann, G., Humphrey, G. C., Gebert, M. J., Van Trueren, W., Berg-Lyons, D., Keepers, K., Guo, Y., Bullard, J., Fierer, N., Carter, D. O., & Knight, R. (2013). A microbial clock provides an accurate estimate of the postmortem interval in a mouse model system. *eLife, 2*, e01104. https://doi.org/10.7554/eLife.01104

Nazari, M. T., Machado, B. S., Marchezi, G., Crestani, L., Ferrari, V., Colla, L. M., & Piccin, J. S. (2022). Use of soil actinomycetes for pharmaceutical, food, agricultural, and environmental purposes. *3 Biotech*, *12*(9), 232. https://doi.org/10.1007/s13205-022-03307-y

Procopio, N., Ghignone, S., Williams, A., Chamberlain, A., Mello, A., & Buckley, M. (2019). Metabarcoding to investigate changes in soil microbial communities within forensic burial contexts. *Forensic Science International: Genetics, 39,* 73-85. https://doi.org/10.1016/j.fsigen.2018.12.002

R Core Team. (2021). *R: A Language and Environment for Statistical Computing*, R Foundation for Statistical Computing, Vienna, Austria.

Rayment, G. E., & Lyons, D. J. (2011). *Soil chemical methods: Australasia, Volume 3*. CSIRO Publishing.

Robeson II, M. R., O'Rourke, D. R., Kaehler, B. D., Ziemski, M., Dillon, M. R., Foster, J. T., & Bokulich, N. A. (2020). RESCRIPt: Reproducible sequence taxonomy reference database management for the masses. *bioRxiv*. https://doi.org/10.1101/2020.10.05.326504

Singh, B., Minick, K. J., Strickland, M. S., Wickings, K. G., Crippen, T. L., Tarone, A. M., Benbow, M. E., Sufrin, N., Tomberlin, J. K., & Pechal, J. L. (2018). Temporal and spatial impact of human cadaver decomposition on soil bacterial and arthropod community structure and function. *Frontiers in microbiology*, *8*, 2616. https://doi.org/10.3389/fmicb.2017.02616

State Government of NSW & Department of Planning, Industry and Environment (NSW DPIE). (2012). *Australian Soil Classification (ASC) soil type map of NSW*. Retrieved May 19, 2025, from https://datasets.seed.nsw.gov.au/dataset/australian-soil-classification-asc-soil-type-map-of-nsweaa10

Taylor, L. S., Mason, A. R., Hauther, K. A., Flores, R., & DeBruyn, J. M. (2024). Transient hypoxia drives soil microbial community dynamics and biogeochemistry during human decomposition. *FEMS Microbiology Ecology, 100*(10), fiae119. https://doi.org/10.1093/femsec/fiae119

Vázquez-Baeza, Y., Pirrung, M., Gonzalez, A., & Knight, R. (2013). Emperor: a tool for visualizing high-throughput microbial community data. *Gigascience*, *2*(1), 16. https://doi.org/10.1186/2047-217X-2-16

Weiss, S., Xu, Z. Z., Peddada, S., Amir, A., Bittinger, K., Gonzalez, A., Lozupone, C., Zaneveld, J. R., Vázquez-Baeza, Y., Birmingham, A., Hyde, E. R., & Knight, R. (2017). Normalization and microbial differential abundance strategies depend upon data characteristics. *Microbiome*, *5*, 27. https://doi.org/10.1186/s40168-017-0237-y

Zhang, J., Wang, M., Qi, X., Shi, L., Zhang, J., Zhang, X., & Yan, J. (2021). Predicting the postmortem interval of burial cadavers based on microbial community succession. *Forensic Science International: Genetics, 52*, 102488. https://doi.org/10.1016/j.fsigen.2021.102488

Supplemental File S1: All soil parameters across cohorts

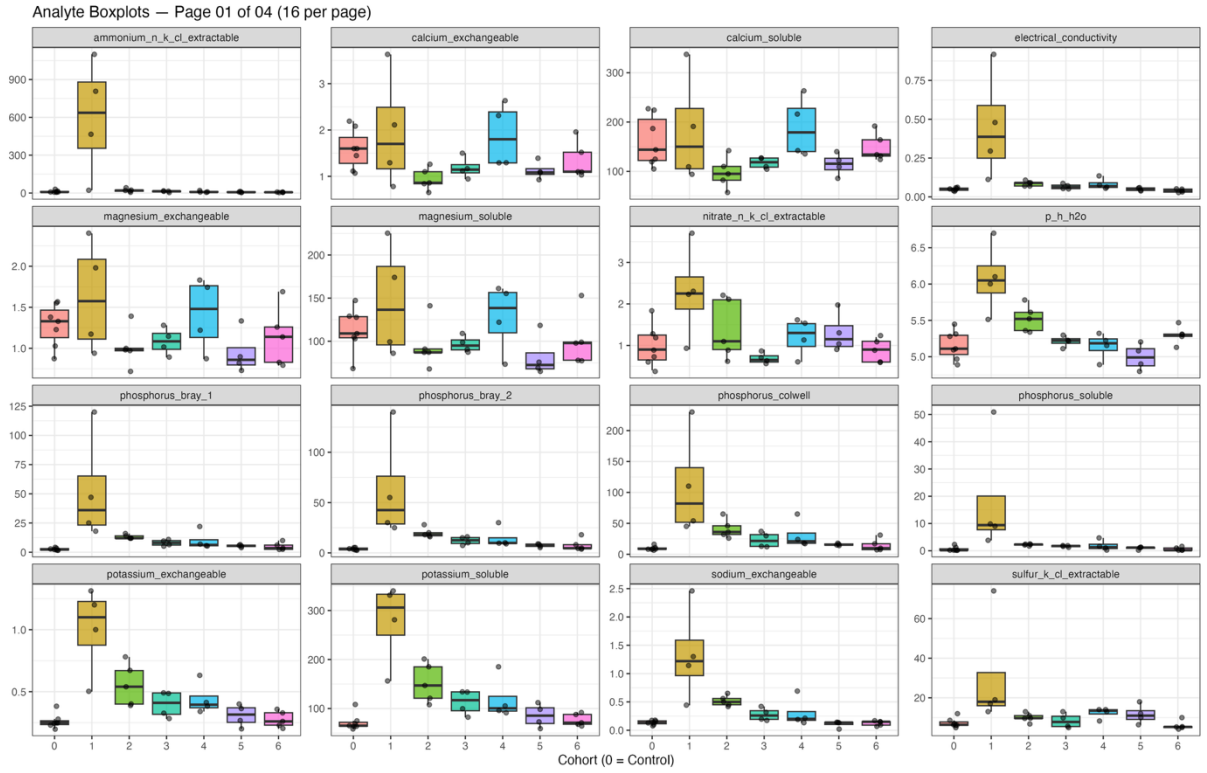

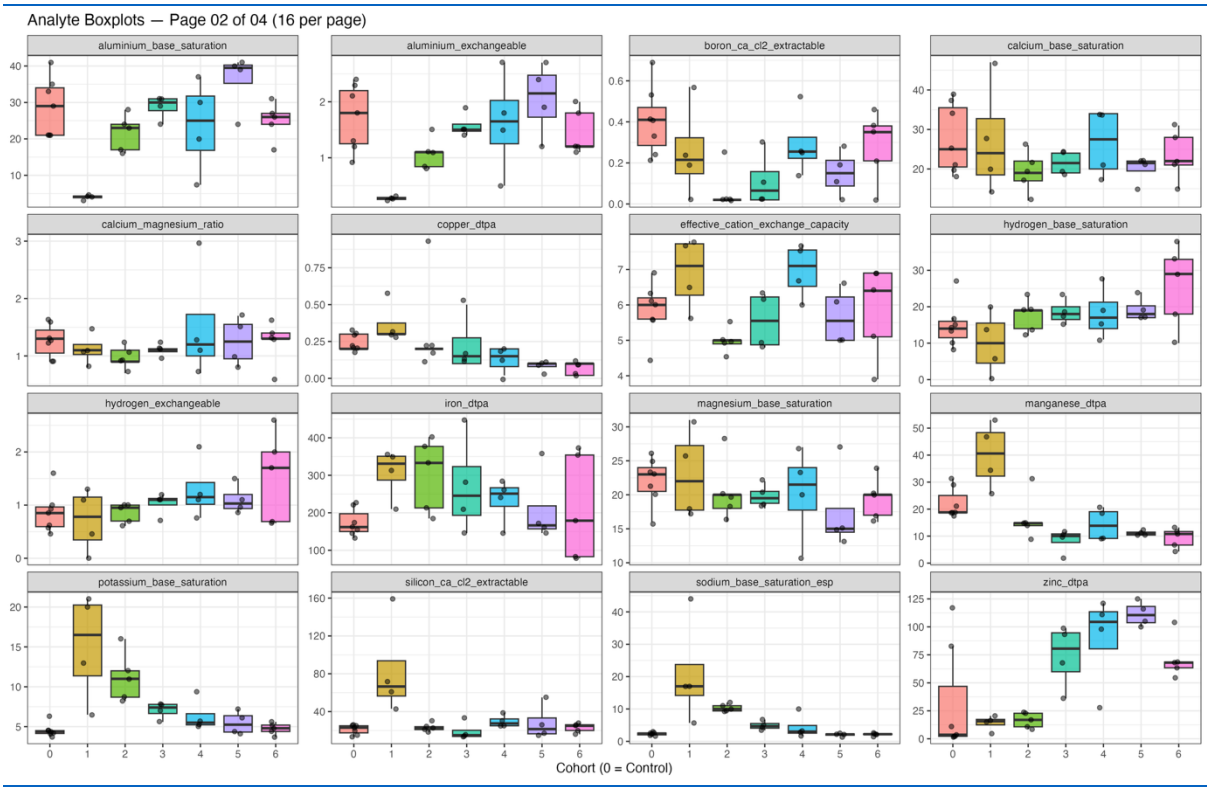

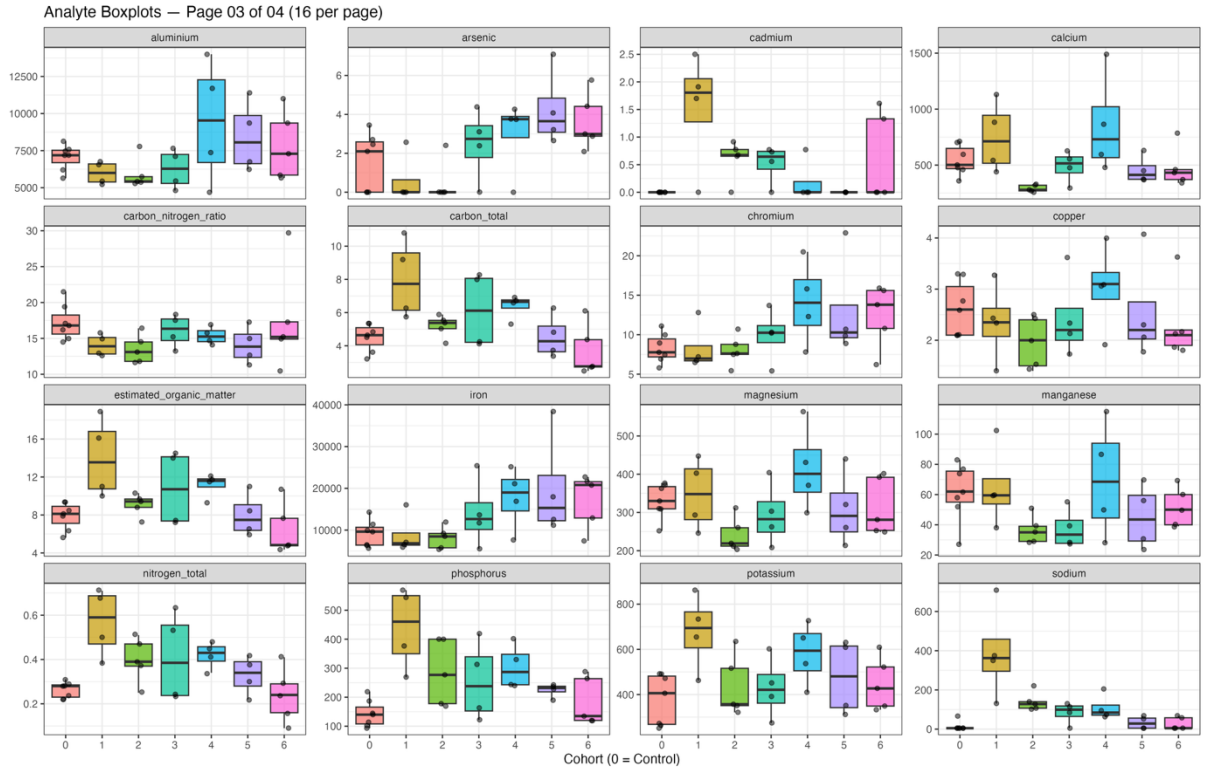
Analyte Boxplots — Page 03 of 04 (16 per page)
aluminium
arsenic
cadmium
calcium
carbon_nitrogen_ratio
carbon_total
chromium
copper
estimated_organic_matter
iron
magnesium
manganese
nitrogen_total
phosphorus
potassium
sodium
Cohort (0 = Control)

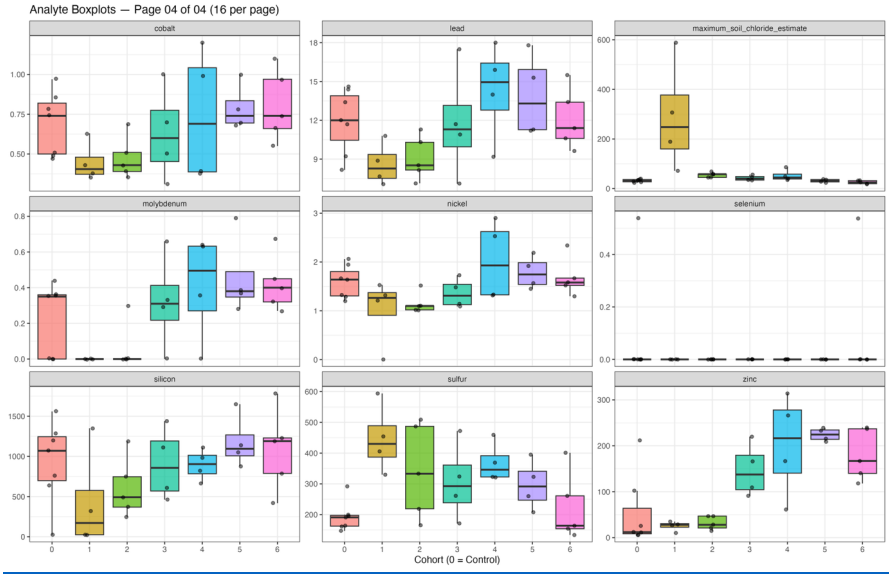
Analyte Boxplots — Page 04 of 04 (16 per page)
cobalt
lead
maximum_soil_chloride_estimate
molybdenum
nickel
selenium
silicon
sulfur
zinc
Cohort (0 = Control)

644 **Supplemental File S2:** Pearson correlation analysis for mean soil parameters

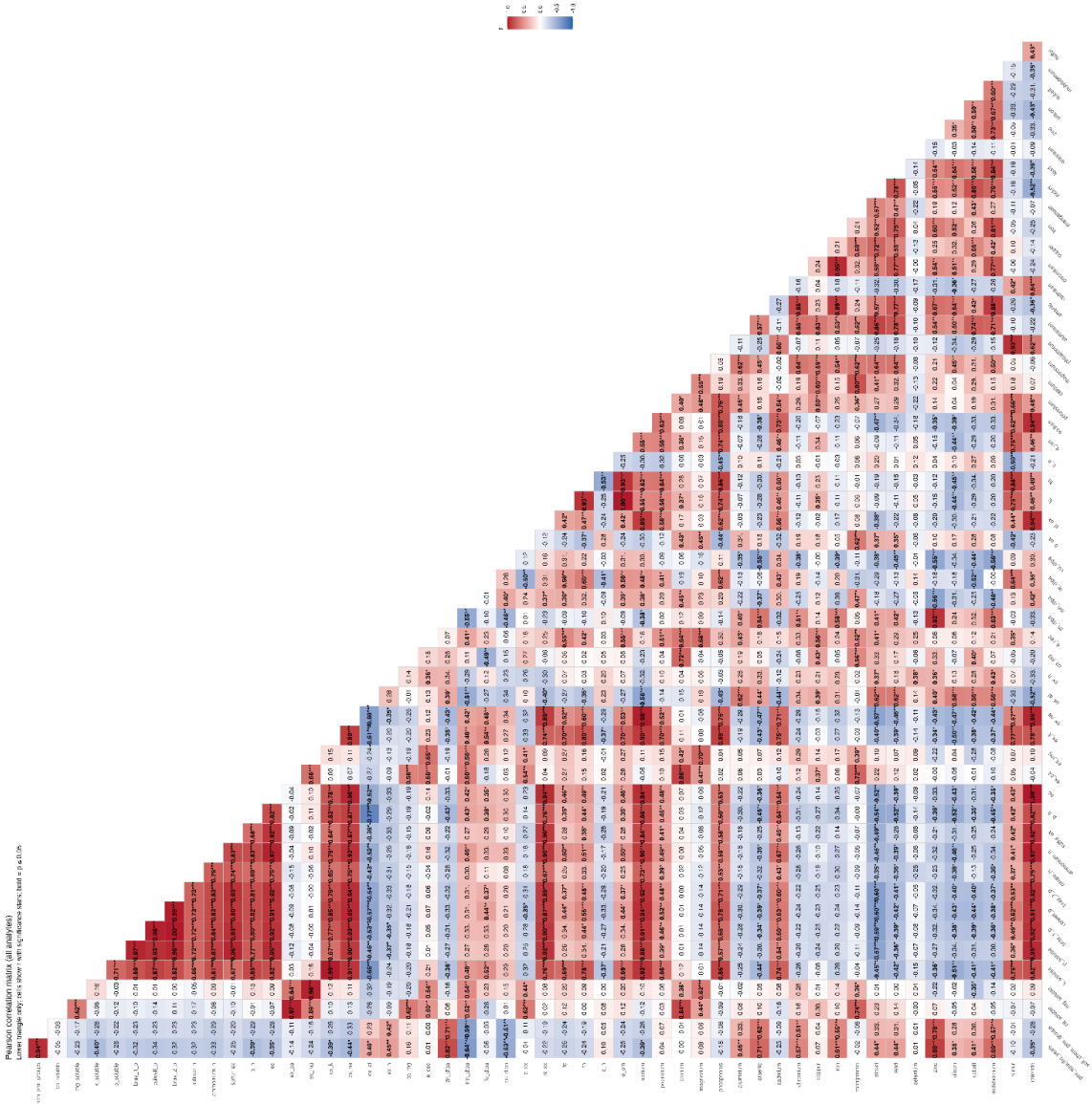

645

Supplemental File S3. Details of DNA extraction for peat samples from AFTER plots, including DNA yield, and 260/230 and 260/280 ratios. Non-composite samples are indicated by an asterisk (*).

Sample ID	DNA Yield ng/µL)	260/230	260/280
A_01_H	112.963	0.53	1.96
A_01_01_H	62.271	-	-
A_03_H	67.469	-	-
A_01_04_S*	79.202	1.49	1.87
A_01_04_H	73.066	1.03	1.89
A_03_03_H	59.605	0.17	1.85
A_04_02_H	73.348	-	-
A_04_04_H	68.398	-	-
A_05_H	80.03	-	-
A_05_01_H	97.47	0.1	1.84
A_05_02_H	24.172	-	-
A_06_01_H	65.363	0.12	1.82
A_06_02_H	152.597	0.49	1.84
A_06_04_H	140.403	-	-
A_07_H	46.072	0.22	1.77
A_07_03_H	98.051	0.82	1.81
A_11_01_H	91.644	0.37	1.82
A_11_03_H	187.185	-	-
A_11_04_H	68.452	1.65	1.8
A_12_01H	41.195	0.81	1.74
A_12_03_H	110.669	-	-
A_12_04_H	108.568	0.38	1.88
A_16_01_H	79.423	0.85	1.79
A_17_04_H	51.119	0.75	1.66
A_18_02_H	55.468	0.96	1.77
A_19_02_H	93.144	1.01	1.81
A_19_04_S*	24.594	0.8	1.76
A_19_04_H	138.88	0.52	1.85
A_22_01_H	119.669	0.78	1.86

A_22_02_H	265.638	-	-
A_24_01_H	169.295	0.33	1.86
A_24_03_H	183.923	1.53	1.89
A_24_04_H	105.808	0.91	1.83
A_31_02_W*	120.741	0.27	1.84
A_31_02_H	216.014	0.65	1.88

650

Supplemental File S4. Details of data processing and Illumina amplicon sequencing for AFTER samples.Non-composite samples are indicated by an asterisk (*).

sample-id	input	filtered	percentage of input passed filter	denoised	merged	percentage of input merged	non-chimeric	percentage of input non-chimeric
#q2:types	numeric	numeric	numeric	numeric	numeric	numeric	numeric	numeric
A-01-01-H	119202	98198	82.38	90664	76584	64.25	73581	61.73
A-01-04-H	123285	103428	83.89	95864	82948	67.28	79114	64.17
A-01-04-S*	132801	110348	83.09	102018	86287	64.97	83099	62.57
A-01-H	78163	65431	83.71	60169	50519	64.63	48528	62.09
A-03-03-H	119495	99196	83.01	92829	81171	67.93	77992	65.27
A-03-H	88419	73465	83.09	68488	59758	67.59	57881	65.46
A-04-02-H	91661	75841	82.74	71013	61533	67.13	58999	64.37
A-04-04-H	107430	88591	82.46	82816	71470	66.53	68932	64.16
A-05-01-H	97038	81366	83.85	75623	65840	67.85	63138	65.07
A-05-02-H	118331	91908	77.67	86336	72311	61.11	69882	59.06
A-05-H	97913	82011	83.76	76505	65616	67.01	63083	64.43
A-06-01-H	109	42	38.53	2	2	1.83	2	1.83
A-06-02-H	84103	69477	82.61	63913	54144	64.38	51461	61.19
A-06-04-H	100367	82889	82.59	76929	66534	66.29	64019	63.78
A-07-03-H	118083	97112	82.24	89751	76709	64.96	74033	62.7
A-07-H	129758	108724	83.79	102538	89387	68.89	85092	65.58

A-11-01-H	107378	89572	83.42	82842	70886	66.02	68185	63.5
A-11-03-H	99697	82140	82.39	75532	64340	64.54	62180	62.37
A-11-04-H	137786	106315	77.16	99238	83543	60.63	80343	58.31
A-12-01-H	109173	89879	82.33	83726	72850	66.73	70054	64.17
A-12-03-H	98238	81152	82.61	74097	61541	62.64	59289	60.35
A-12-04-H	105841	88020	83.16	81570	70102	66.23	66351	62.69
A-16-01-H	128034	106136	82.9	99410	87184	68.09	83026	64.85
A-17-04-H	96635	78920	81.67	74420	65649	67.94	61356	63.49
A-18-02-H	124772	103991	83.34	97323	85778	68.75	81016	64.93
A-19-02-H	82484	67776	82.17	62401	52533	63.69	50673	61.43
A-19-04-H	110130	87689	79.62	81956	69419	63.03	63213	57.4
A-19-04-S*	127133	105594	83.06	99934	88520	69.63	79464	62.5
A-22-01-H	121390	100297	82.62	94529	84100	69.28	76926	63.37
A-22-02-H	89170	74028	83.02	70796	63702	71.44	54199	60.78
A-24-01-H	81151	67757	83.49	63755	57626	71.01	52806	65.07
A-24-03-H	72891	60278	82.7	56088	49552	67.98	45043	61.8
A-24-04-H	100044	83979	83.94	78328	70409	70.38	67505	67.48
A-31-02-H	91793	76142	82.95	73914	66265	72.19	52326	57
A-31-02-W*	134656	103366	76.76	99381	90149	66.95	78631	58.39
A-31-04-H	90388	74447	82.36	70355	62435	69.07	53211	58.87

654

Supplemental File S5. Alpha diversity analysis (observed features) conducted using QIIME2 for the microbial community at AFTER (*n*=7 plots) for the cohort 0 (control; six samples), cohort 1 (1 year PMI; five samples), cohort 2 (1-2 years PMI; seven samples), cohort 3 (4-5 years PMI; four samples), cohort 4 (7 years PMI; three samples), cohort 5 (8 years PMI; four samples) and cohort 6 (9 years PMI; six samples). Differences in alpha-diversity (ASV richness) were calculated using a Kruskal-Wallis test.

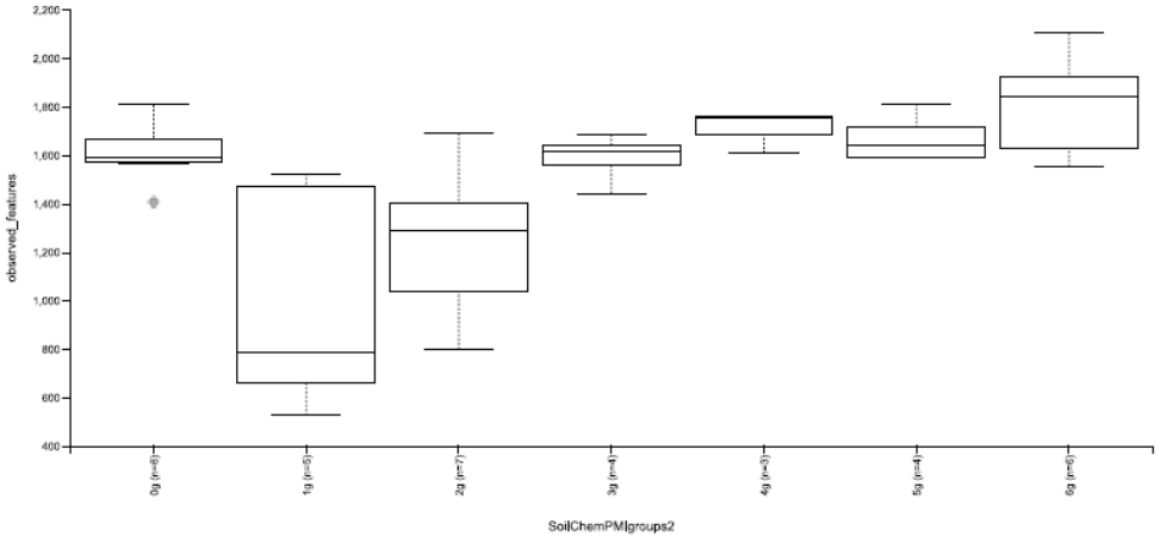

Kruskal-Wallis (all groups)

	Result
H	19.37961899425692
p-value	0.003568314620742333

Supplemental File S6. Alpha diversity analysis (Shannon Index) conducted using QIIME2 for the microbial community at AFTER (*n*=7 plots) for the cohort 0 (control; six samples), cohort 1 (1 year PMI; five samples), cohort 2 (1-2 years PMI; seven samples), cohort 3 (4-5 years PMI; four samples), cohort 4 (7 years PMI; three samples), cohort 5 (8 years PMI; four samples) and cohort 6 (9 years PMI; six samples). Differences in alpha-diversity (ASV richness) were calculated using a Kruskal-Wallis test.

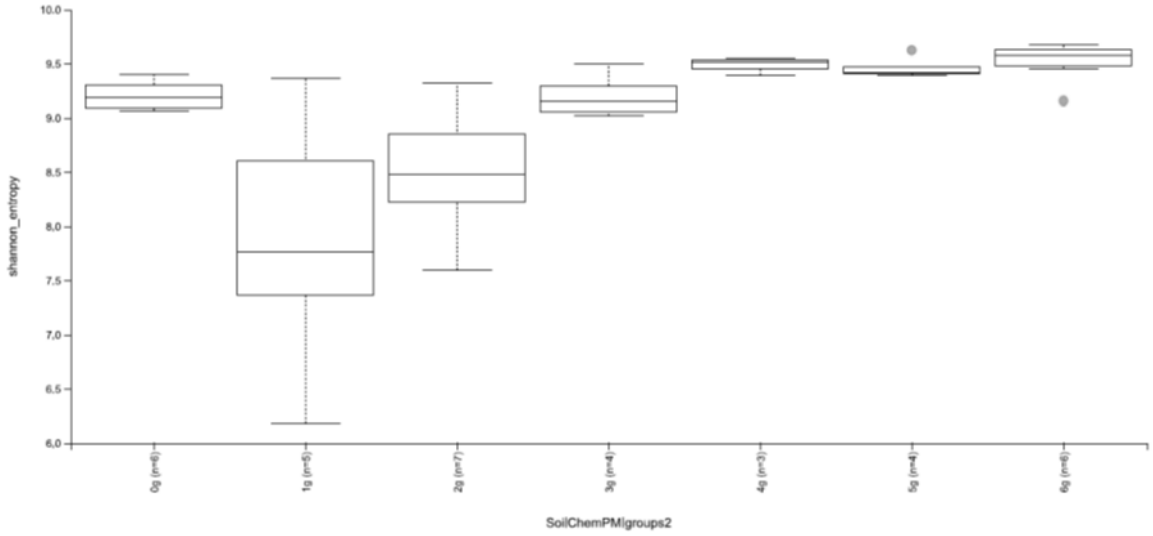

Kruskal-Wallis (all groups)

	Result
H	24.079229024943317
p-value	0.0005050194218573775

680 **Supplemental File S7.** Details of alpha diversity (Pielou evenness) analysis conducted in
681 QIIME2 forAFTER plot samples. Non-composite samples are indicated by an asterisk (*).

682

Sample ID	Pielou evenness
#q2:types	numeric
A-01-01-H	0.89
A-01-04-H	0.88
A-01-04-S*	0.88
A-01-H	0.87
A-03-03-H	0.89
A-03-H	0.87
A-04-02-H	0.90
A-04-04-H	0.86
A-05-01-H	0.89
A-05-02-H	0.88
A-05-H	0.85
A-06-02-H	0.88
A-06-04-H	0.88
A-07-03-H	0.89
A-07-H	0.84
A-11-01-H	0.89
A-11-03-H	0.89
A-11-04-H	0.89
A-12-01-H	0.89
A-12-03-H	0.88
A-12-04-H	0.87
A-16-01-H	0.85
A-17-04-H	0.86
A-18-02-H	0.87
A-19-02-H	0.89
A-19-04-H	0.82
A-19-04-S*	0.84
A-22-01-H	0.82

A-22-02-H	0.79
A-24-01-H	0.82
A-24-03-H	0.82
A-24-04-H	0.85
A-31-02-H	0.68
A-31-02-W*	0.79
A-31-04-H	0.81
A-01-01-H	0.89